Journal of Zhejiang University-SCIENCE A (Applied Physics & Engineering) 2024 25(12):991-1005
www.jzus.zju.edu.cn; www.springer.com/journal/11582
E-mail: jzus_a@zju.edu.cn

Research Article
https://doi.org/10.1631/jzus.A2400354

Waterproofing performance of longitudinal segmental tunnel joints under external loads: a full-scale experimental investigation

Dongmei ZHANG[1,2]✉, Sirui CHEN[2], Zhongkai HUANG[1,2]✉, Zhaoyuan ZHANG[2], Long SU[3]

[1]*Key Laboratory of Geotechnical and Underground Engineering of Ministry of Education, Tongji University, Shanghai 200092, China*
[2]*Department of Geotechnical Engineering, College of Civil Engineering, Tongji University, Shanghai 200092, China*
[3]*Chine Railway 14th Bureau Group Mega Shield Construction Engineering Corporation Limited, Jinan 250014, China*

Abstract: When subjected to external loads from the ground and nearby construction, tunnel segmental lining joints are prone to damaging deformation. This can result in water leakage into tunnels, posing great safety risks. With this issue in mind, we conducted a series of full-scale tests to study the effects of external loads on the waterproofing performance of longitudinal joints. A customized rig for testing segmental joints was developed to assess the effect of loading magnitude, eccentricity, and loading-unloading-reloading cycles on waterproofing performance. Additionally, the relationship between joint force, sealing gasket deformation, and waterproofing pressure was investigated. The results indicate that: (1) the sealing gasket's compression rapidly decreases as external loads increase, which weakens the waterproofing capacity of the joint; (2) the watertightness limit dramatically decreases as the bending moment increases; (3) a loading-unloading-reloading cycle leads to degradation of the joint's waterproofing performance. The findings of this study provide a reference for subsequent waterproofing design of segmental tunnel joints, helping ensure the safety of tunnels throughout their operational lifespans.

Key words: Segmental tunnel; Waterproofing performance; Full-scale experiment; Longitudinal joint

1 Introduction

Shield tunneling technology is extensively used in tunnel construction due to its efficiency and safety (Kasper and Meschke, 2006; Huang et al., 2021, 2024; Zhang et al., 2022a). However, precast concrete segments form the majority of the tunnel linings, and many joints between them eventually become leakage channels. As a result, tunnel leakage is commonly observed at longitudinal and circumferential segmental joints (Shen et al., 2014; Huang et al., 2018; Wu et al., 2020), as shown in Fig. 1. Water leakage is a long-term issue, and leakage-induced problems have become a significant concern in tunnel engineering (Zhou et al., 2021). Moreover, in low permeability soils, tunnel leakage creates a new drainage boundary, potentially resulting in ground and tunnel settlements (Zhang et al., 2015). In highly permeable soils, such as sands or silty sands, water leakage can lead to internal erosion, resulting in ground loss or adverse effects to the stress performance of the tunnel structure (Zhang et al., 2019; Li et al., 2021). These leakage-caused issues can reduce the safety of the tunnel during its operational life (Zheng et al., 2017; Zhang et al., 2022a).

The common understanding regarding waterproofing performance of tunnels is that the capability to prevent water leakage at joints mainly depends on sealing gaskets (Xu et al., 2016; Zhang et al., 2021a; Zhang DM et al., 2022b). However, environmental disturbances, such as surcharge or excavation above the tunnel, frequently occur in urban areas during the operation of segmental tunnels (Shalabi et al., 2016; Lin et al., 2022). Additionally, when subjected to unexpected external loads, segmental joints are susceptible to unfavorable deformations, which can lead to tunnel leakage (Wu et al., 2023). In particular, loading-unloading-reloading

✉ Dongmei ZHANG, dmzhang@tongji.edu.cn
Zhongkai HUANG, 5huangzhongkai@tongji.edu.cn
Sirui CHEN, https://orcid.org/0009-0000-8999-546X

Received July 11, 2024; Revision accepted Sept. 27, 2024; Crosschecked Dec. 2, 2024

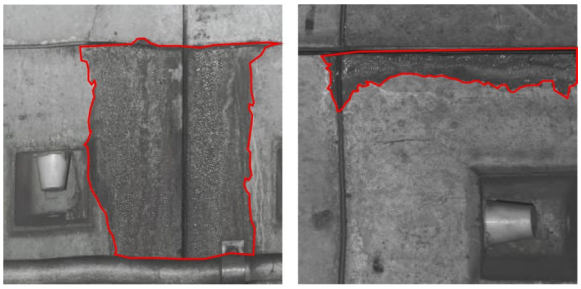

Fig. 1 Leakage in segmental tunnels: (a) at a circumferential joint; (b) at a longitudinal joint

cycles can cause degradation of the joint's waterproofing performance. For instance, Chen et al. (2016) identified possible water penetration passages, considering the influence of a large excavation in soft soils on nearby tunnels. Huang et al. (2017) demonstrated the loss of waterproofing at the waist joint of a tunnel due to an unexpected surcharge. Therefore, to ensure the safety and durability of tunnel structures in the face of adjacent disturbances, it is important to investigate the waterproofing performance of tunnel segmental joints under various external loads.

Sealing gaskets play a crucial role in preventing water leakage into tunnels. Numerous studies have been conducted on the gasket itself, including its material (Shen et al., 2014; Yang et al., 2018), aging mechanism (Wang et al., 2021; Li et al., 2023), optimal placement (Petraroia et al., 2024), and form (Gong et al., 2017; Zhang et al., 2018). Furthermore, several researchers have focused on the effect of adjacent concrete segments on the sealing gasket in studying waterproofing performance. For instance, Shalabi et al. (2016) analyzed the gasket load deformation behavior and the sealant capacity using a steel frame device for water leakage tests. Gong et al. (2019) considered the compression of joints and established a relationship between waterproof pressure and the average contact stress of the gaskets. Moreover, Zhang et al. (2022b) analyzed the waterproofing mechanism of gaskets under different joint deformation conditions, particularly focusing on the effect of joint rotation. However, little research has focused on joint forces under various external loads. In particular, the relationship between joint force, sealing gasket deformation, and waterproof pressure has not been established.

Among various research methods, experimental testing is a universal and effective approach to investigating the waterproofing performance of gasketed joints (Zhang et al., 2021b). Generally, laboratory joint leakage tests can be categorized into two types according to the material of the joint: steel (Shalabi et al., 2016) and concrete (Ding et al., 2017). The former is easy to process and operate. However, since gaskets are glued into concrete grooves in practice (Fig. 2), the contact surface characteristics between the two are inconsistent, which may make experimental results unreliable (Gong et al., 2022). In view of the disadvantages of traditional steel structural testing, many researchers have used concrete specimens in testing (Ding et al., 2017; Zhang et al., 2022b). However, relevant experimental studies on sealing gaskets have mainly been performed at small scales. Although this is time-saving and economical, as it simplifies the tunnel segments, the mechanical behavior and geometric characteristics of the lining structure and joints are not properly accounted for. For this reason, Shalabi et al. (2012) evaluated the longitudinal joint sealant behavior under static and dynamic loadings using large-scale straight concrete segments. Compared to a segment with curvature, there are significant differences in the modes of deformation and forces, and the relationship between joint force, joint deformation, and waterproof pressure is not well characterized. Accordingly, Zhang et al. (2021b) proposed a novel full-scale experimental set-up to investigate the waterproofing and mechanical behavior of sealing gaskets for circumferential joints, detecting the leakage process of gaskets in a detailed manner (Zhang et al., 2021a).

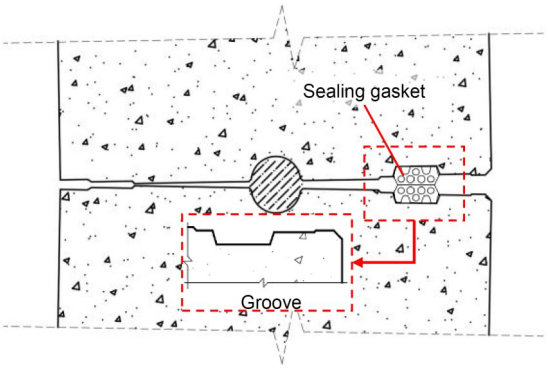

Fig. 2 Schematic of the groove and the sealing gasket

However, in the event of a surcharge, joints located at the crown or invert are subjected to positive bending moments, while the longitudinal joints located along the springline are subjected to negative bending moments (Fig. 3). In Fig. 3, M and N represent bending

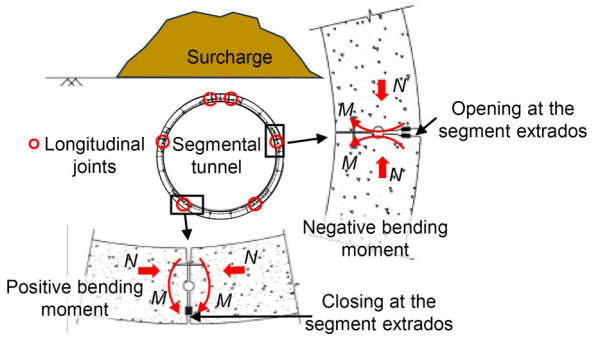

Fig. 3 Schematic of the joint deformation under surcharge

moments and axial forces, respectively. In the negative bending mode, the joint opens at the segment extrados (the side in contact with the soil), and the compression of the sealing gasket decreases more significantly, increasing the possibility of a leak (Huang et al., 2017). Notably, our understanding of the sealing process of longitudinal joints under external loads is limited, especially for joints subjected to negative bending moments.

Given the restrictions described above, a series of full-scale tests are conducted to study the effect of external loads on the waterproofing performance of longitudinal segmental joints under negative bending moments. First, a custom testing rig was developed for concrete segmental joints to account for the effect of load magnitude and eccentricity on waterproofing performance. The impacts of load magnitude, eccentricity, and loading-unloading-reloading cycles on waterproofing performance were then evaluated based on three sets of experimental results. In this way, the relationship between joint force, sealing gasket deformation, and waterproof pressure was investigated.

2 Joint waterproofing test

2.1 Prototype

The typical lining structure used in the Shanghai subway system is adopted in this study. Fig. 4 illustrates the structure of the tunnel segmental ring and its corresponding details. The tunnel segmental ring is characterized by a symmetrical structure with an external diameter of 6.2 m. The thickness and width of the tunnel segment are 0.35 and 1.20 m, respectively. Each segmental ring comprises one key segment (F), two adjacent segments (L1 and L2), two standard segments (B1 and B2), and one inverted segment (D). According to the Chinese national concrete design code (MHURD, 2010), the strength grade and impermeability of the segment concrete are C55 (i.e. having an ultimate compressive strength of 55 MPa) and P10 (i.e. capable of resisting hydrostatic pressure of 1.0 MPa without seepage), respectively. The longitudinal joints and circumferential joints of the segment are connected

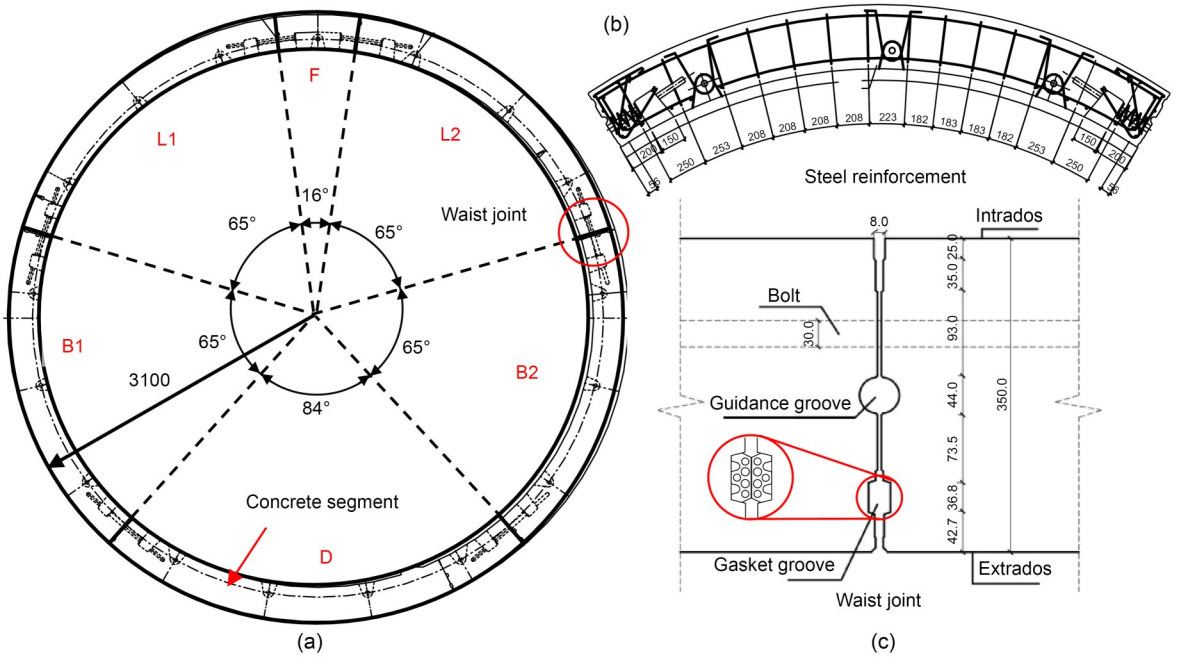

Fig. 4 Prototype of the tunnel (unit: mm): (a) segmental lining; (b) steel reinforcement; (c) waist joint

by straight bolts. Fig. 4 presents a scheme of the steel reinforcement within each concrete segment and depicts detailed joint geometry information. The joint is equipped with a guidance groove and elastic sealing gaskets with a width of 36.8 mm and a height of 16 mm (Fig. 5), which are made of ethylene propylene diene monomer (EPDM).

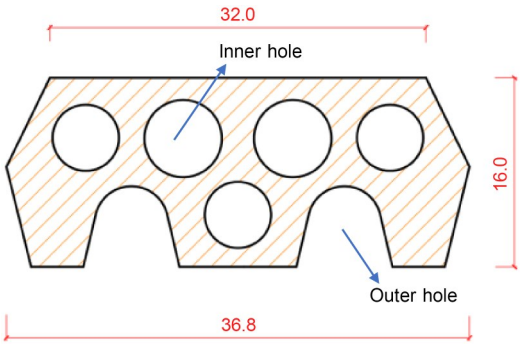

Fig. 5 Details of the sealing gasket (unit: mm)

2.2 Design of the test

A schematic of the test mechanism is shown in Fig. 6. Loading is applied through vertical forces (P) and horizontal axial forces (N) to simulate the stress on the joint. In the diagram, A represents the water storage hole sealed by a gasket, B is the water inlet pipe connected to an automatic hydraulic press, and C is the water outlet pipe sealed at the beginning of the experiment. Under a certain external loading condition, the water pressure is continuously increased under the control of the hydraulic press until leakage occurs at the sealing gasket; at this point, the joint has reached its watertightness limit. Subsequently, the test is continued by modifying the loading conditions to obtain the relationships between the joint force, sealing gasket deformation, and watertightness limit.

Due to the limitations of the loading system, the specimens were cut from the tunnel lining ring, as shown in Fig. 7. After cutting and assembling, the specimen formed an arc with an angle of approximately 48°. The inlet and outlet water pipes were embedded within the concrete during the casting of the segment. Meanwhile, the water pipes were sealed to prevent concrete ingress, as shown in Fig. 8.

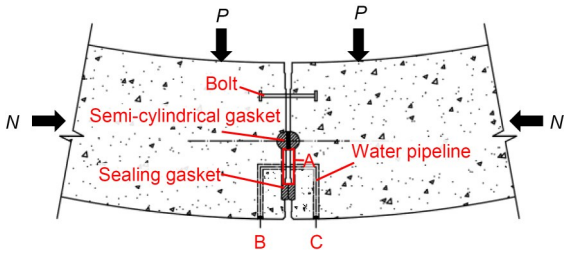

Fig. 6 Schematic of the test mechanism

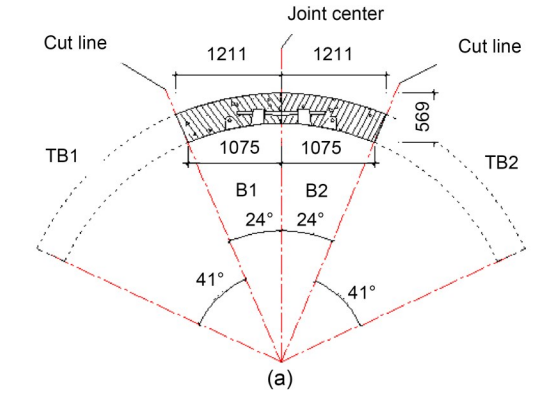

Fig. 7 Schematic diagram of segment cutting: (a) segment cutting plan (unit: mm); (b) on-site segment cutting

The production of the gasket is crucial for the water leakage test. In this study, a special sealing gasket is used to maintain the water pressure in the water storage hole (A in Fig. 6), as shown in Fig. 9a. Its dimensions were determined based on the gasket groove, as shown in Figs. 9b and 9c. In creating the sealing gasket groove, the guidance groove can be used as one edge of the sealing gasket groove. As shown in Fig. 9d, two concrete grooves of the same specifications were cut at appropriate positions perpendicular to the sealing gasket groove, forming the sealing gasket groove required for the test. One semi-cylindrical edge and three sealing edges (one long and two short) made up the entire sealing gasket. The diameter of the

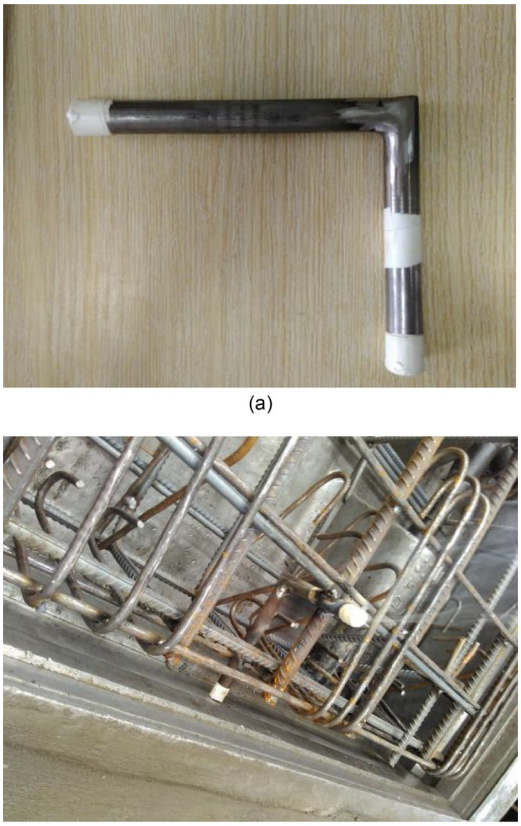

Fig. 8 Water pipes: (a) temporary sealing treatment of water pipe; (b) welding of water pipes to the reinforcement cage

semi-cylindrical edge was 40 mm. Meanwhile, to ensure that water leakage did not occur in the semi-cylindrical part, a "filling part" was added, where the upper surface of the filling part was coplanar with the upper surface of the sealing gasket. The entire sealing gasket and the "filling part" are made of EPDM.

2.3 Testing and measurement system

In full-scale testing, the applied loading should align with the actual stress conditions experienced by the tunnel structure under external loads. Ground surcharge or unloading can impact the internal force distribution of tunnel structures, especially in shallow tunnels. Under the action of a surcharge above the tunnel, longitudinal joints will experience significant bending moments (M) and axial forces (N). Additionally, ground unloading can influence the mechanical and waterproofing performance of the joints.

By using an analytical joint model of a segmental tunnel based on the multi-hinge ring calculation method (Lee and Ge, 2001) or the modified routine method (Koyoma and Nishimura, 1998), the values of M, N, and M/N (i.e., eccentricity) at tunnel joints can be calculated under various geological conditions and external loads. In this study, different eccentricities and axial forces were applied to investigate the impact of external loads. The surcharge condition was simulated

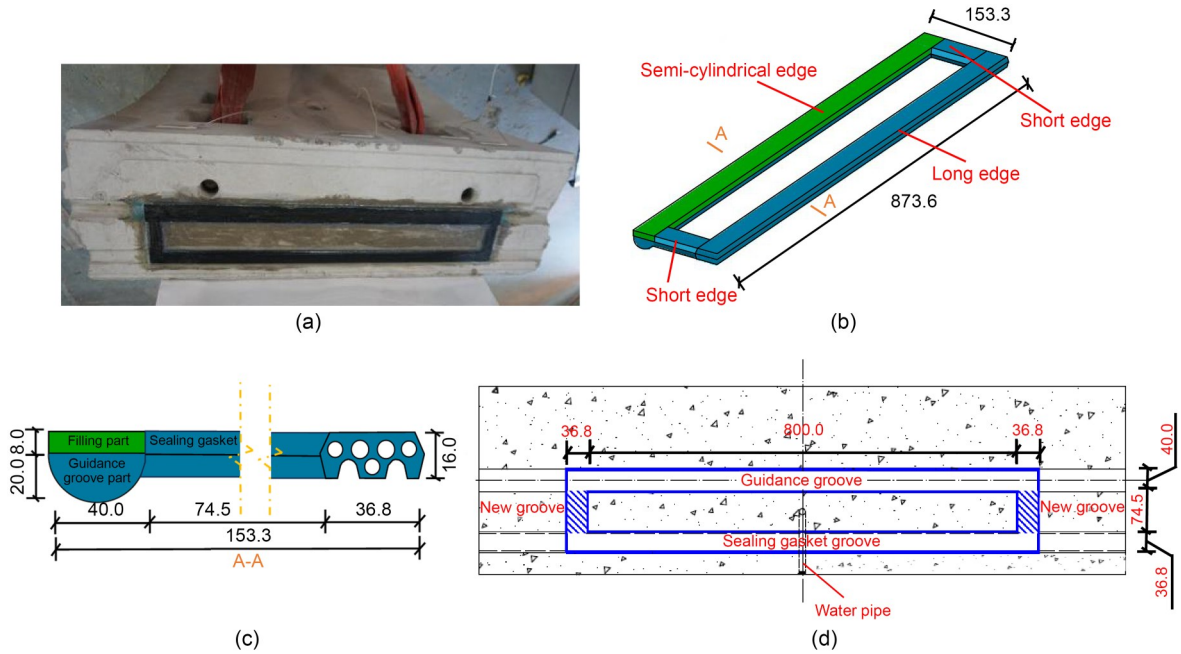

Fig. 9 Sealing gasket: (a) photograph of the sealing gasket; (b) 3D schematic of the sealing gasket (unit: mm); (c) side view of the sealing gasket (unit: mm); (d) sealing gasket groove (unit: mm)

by applying axial forces at the joint under specific eccentric conditions, and the unloading condition was simulated by removing these forces. Therefore, the testing rig was capable of controlling the eccentricity and axial force of the joints.

Fig. 10 illustrates the testing rig for waterproofing performance tests. Generally, the rig consists of three components: (a) the loading system, which included horizontal and vertical hydraulic jacks; (b) steel brackets with steel rollers, which formed a roller bearing condition with low friction; (c) the test specimen, which included two concrete specimens and a sealing gasket. Fig. 11 illustrates the loading diagram. In this regard, horizontal and vertical hydraulic jacks were set to correspond with the actual force applied to the joint. The relationship between the external vertical force, axial force, and bending moment in the joint section is shown in Eq. (1):

$$M=P\cdot(L_3-L_1)+G\cdot(L_2-L_1)-N\cdot h, \qquad (1)$$

where N represents the axial force applied by the hydraulic jack, which is equivalent to the axial force on the tunnel joint; P represents the external vertical force; M denotes the joint bending moment. Therefore, the external vertical force (P) can be adjusted to change the eccentricity (e) of the joint under specific external horizontal loading conditions: L_1=1190 mm, L_2=595 mm, L_3=400 mm, and h=250 mm; F_R is the support force; G is the segment weight, which is 12.6 kN. These variables are shown in Fig. 11.

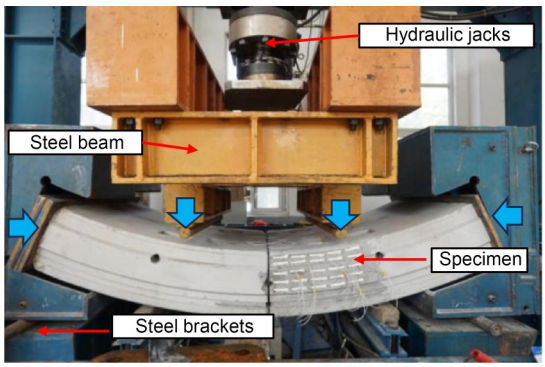

Fig. 10 Testing system diagram

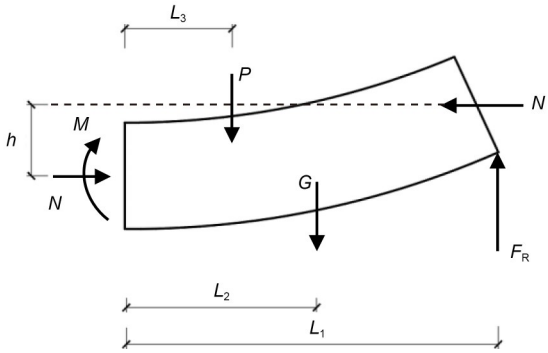

Fig. 11 Loading diagram of a specimen

During testing, particular attention was paid to the deformation of the joint. The extrados joint opening, intrados joint opening, and opening at the sealing gasket were measured by linear variable differential transducers (LVDTs). The details of the measurement program are listed in Table 1, and measurement points of the LVDTs are illustrated in Fig. 12, where the segments unfold along one side for better visualization. Two measurement points were used to monitor the opening at the sealing gasket and the extrados joint opening. The monitoring results were represented by their average value. Additionally, a ZH-201 automatic hydraulic press was used to set the water pressure. This apparatus utilizes a pressure sensor to input pressure signals into the system, which automatically controls the start and stop of the water pump based on the actual pressure value, maintaining a constant pressure. During the test, the main variables observed included displacement, time, and the amount of water leakage. Due to spatial limitations, the water leakage was measured using a semi-qualitative method. Water leakage was

Table 1 Summary of the details of the measurement program

Symbol	Number	Measurement location
●	H5, H10	Opening at the sealing gasket
▬	H11	Intrados joint opening
▲	H1, H12	Extrados joint opening

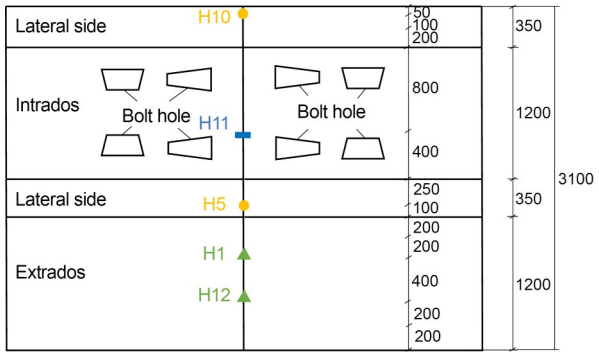

Fig. 12 Test measurement point layout diagram (unit: mm)

categorized into three levels: start of leaking (one drip every 3–5 s), continuous leaking (3–5 drips/s), and watertightness limit (0.08 L/min, where the outflow equals the inflow). In this study, the watertightness limit value is considered to represent the waterproofing capacity of the joint under the given external loading condition.

2.4 Test cases and procedure

The design of the test scheme is summarized in Table 2. The influence of external loads on the waterproofing performance of longitudinal joints, with regards to eccentricity, magnitude, and loading-unloading-reloading effects, are investigated in subsequent tests. According to existing full-scale ring tests (Liu et al., 2016) and numerical simulations (Zhao et al., 2017) of the ultimate strength of tunnel linings, the eccentricity is about 0.15 m for a longitudinal joint. Considering that the eccentricity of the longitudinal joint located along the springline will change under different loading conditions, our tests used three values of eccentricity: e=0.15, 0.20, and 0.25 m. Among these, incremental loading was used for cases with an eccentricity of 0.15 m. For the other two cases, loading-unloading-reloading tests were conducted initially, followed by incremental loading until specimen failure.

Table 2 Test cases

Test case	Eccentricity, e	Loading course
Case 1	0.15 m	Incremental loading
Case 2	0.20 m	Loading-unloading-reloading cycle
Case 3	0.25 m	Loading-unloading-reloading cycle

Fig. 13 summarizes the joint waterproofing test procedures. The joint waterproofing test starts after the completion of the sealing gasket installation, segment assembly, and other preparatory steps. The axial force N is increased in incremental steps with a magnitude of 50 kN. If the vertical jack displacement is unstable during one loading step, which indicates that the concrete is approaching its strength limit, the increment is reduced to 25 kN. The bending moment M is controlled by the equation M=N·e. The waterproofing performance of the joint is monitored simultaneously with its deformation. The deformation of the joint is measured at each increment, and the waterproof pressure is measured every two increments. While measuring waterproof pressure, water flows from the automatic hydraulic press through the water inlet pipe (B) into the water storage hole (A) (Fig. 6). The pressure from

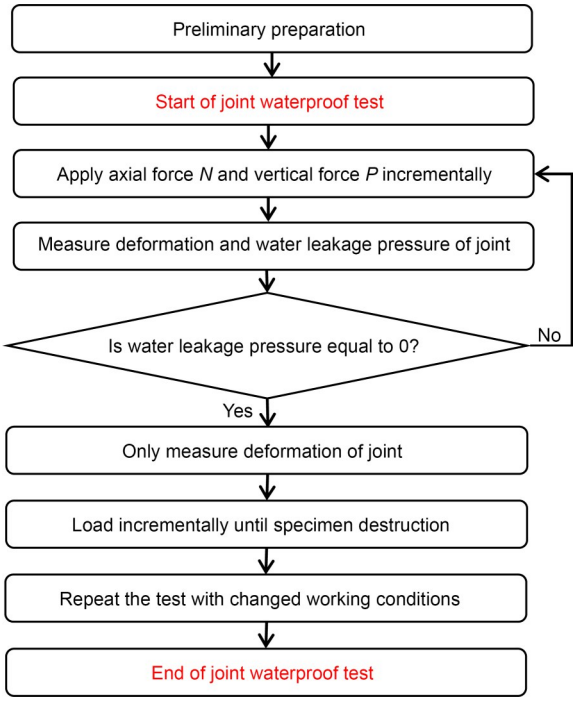

Fig. 13 Test procedure for the joint waterproofing test

the automatic hydraulic press increases at a rate of 0.1 MPa/min until water flows through the sealing gasket, reaching the watertightness limit. This pressure represents the waterproof pressure under a specific external loading condition.

Continuous monitoring of the test is conducted to observe the development of leakage and record the waterproof pressure. A waterproof pressure of 0 indicates a loss of waterproofing function, meaning the joint has reached its ultimate waterproofing capability (i.e. it is no longer watertight). After this point, waterproof pressure is no longer measured as the external loads increase. However, the joint deformation continues to be measured until specimen failure. In Cases 2 and 3, external loads are gradually unloaded along the original path until reaching 0, and then this is followed by reloading. The loading process is illustrated in Fig. 14 with Case 2 as an example. Joint deformation and waterproof pressure are monitored during the reloading process, as done previously.

3 Experimental results and discussion

3.1 Evolution of the waterproof pressure

Our experimental observations indicate that as water pressure increases for a given load magnitude,

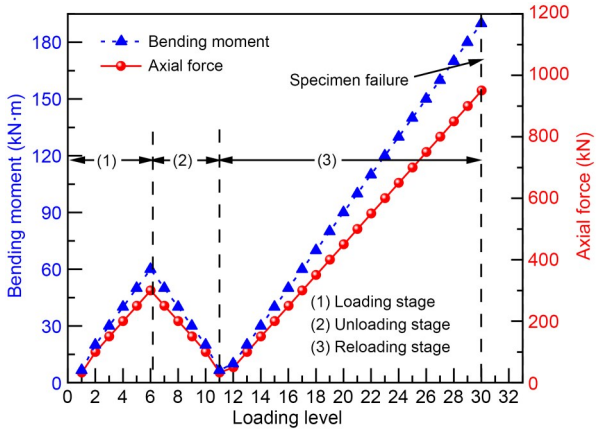

Fig. 14 Loading process in Case 2 (e=0.20 m)

the joint initially starts leaking, followed by continuous dripping, and eventually progresses to water spraying, which indicates the watertightness limit has been reached. Fig. 15 illustrates the relationship between waterproof pressure and axial force for different eccentricities. The dashed line represents the water pressure at which leakage begins for the joint, while the solid line represents the water pressure at which water spraying occurs under different axial forces. In each test case, the waterproof pressure decreases with an increase in external loads. As shown in Fig. 15, the waterproofing performance of the joint decreases sharply in the early stages of loading (N<200 kN) and gradually trends to 0. This observation may be due to the nonlinear deformation of the sealing gasket that occurs with the increase in external loads. This will be investigated further in Section 3.4.

Regardless of the size of the external loads, when the sealing gasket starts to leak (approximately one drip every 3–5 s), a slight increase in external loads is enough for the joint to reach its watertightness limit, as shown in Fig. 15. Moreover, these two curves gradually converge as the axial force increases. This phenomenon may be caused by the formation of a leakage path at the gasket-to-gasket interface or gasket-to-groove interface when the joint starts to leak, as shown in Fig. 16. Accordingly, this seepage path becomes a weak point in the entire gasket. The sealing gasket soon reaches its watertightness limit due to the rapid expansion of the seepage channel caused by increased water pressure or additional joint opening. As a result, the joints exhibiting initial leakage are extremely sensitive to external loads, and this sensitivity grows with increasing external pressure. Thus, the joint will quickly exceed its watertightness limit if external environmental circumstances change, such as rising groundwater levels or surcharges.

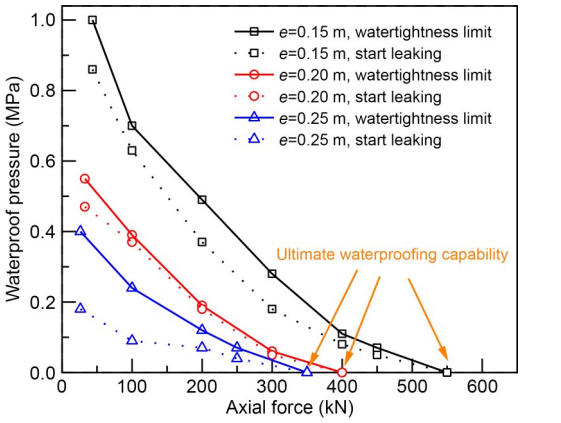

Fig. 15 Waterproof pressure-load relationship of the joint under different eccentricities

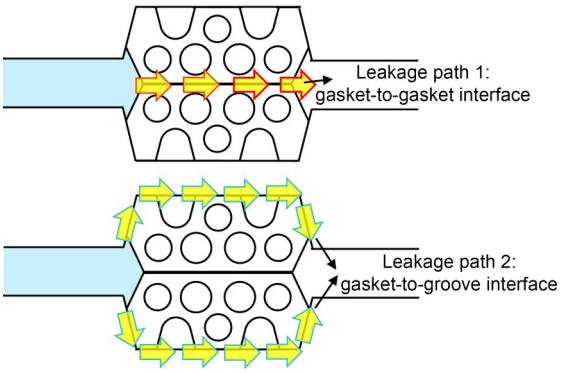

Fig. 16 Leakage path diagram

A larger eccentricity in the joint corresponds to a greater bending moment under the same axial force conditions, resulting in more severe joint deformation. Comparing different eccentricities, the waterproof pressure decreases as the eccentricity increases throughout the entire loading process. This decrease in waterproof pressure is more evident at lower axial forces (N<100 kN), while for N levels beyond 250 kN, the effect of eccentricity on waterproof pressure is minor. Correspondingly, the axial force significantly decreases as the eccentricity increases when the ultimate waterproofing capability is reached. Specifically, the axial forces corresponding to the ultimate waterproofing capability are 550, 400, and 350 kN for eccentricities of 0.15, 0.20, and 0.25 m, respectively. This indicates that the larger the eccentricity, the more susceptible the joint is to waterproofing failure under external loads.

Therefore, the joint moment is a crucial factor affecting the waterproofing performance.

3.2 Effect of a loading-unloading-reloading cycle on the waterproofing performance

In the experiments with eccentricities of 0.20 and 0.25 m, a leakage water test was conducted under one cycle of loading. Based on these results, the relationship between the axial force and the watertightness limit during the loading process is depicted in Fig. 17. It is observed that there is a significant reduction in the joint's waterproofing performance during reloading. Specifically, the ultimate watertightness limit of the joint decreases by approximately 50% during reloading compared to initial loading at the same load level. Analyzing the experimental process reveals two main factors for the decrease in the joint's waterproofing performance under one cycle of loading.

(1) The primary cause of the decrease in waterproofing performance is the increased sealing gasket deformation caused by the loading-unloading-reloading cycle. Monitoring of the sealing gasket deformation showed that even after unloading, the deformation was not fully reversible. For example, Fig. 18 shows the change in the opening of the sealing gasket during one cycle of loading for Case 2. After unloading, the opening of the sealing gasket did not return to the initial level, but remained at 2.99 mm; the deformation of the sealing gasket only recovered by about 30%. This phenomenon may be attributed to the compression and densification of microcracks in the concrete of the stressed zone during the early loading process. Additionally, the bolts of the joint undergo short-term irreversible elastic or plastic deformation under tension, leading to some unrecoverable openings in the joint. Therefore, these deformations do not completely recover during unloading, resulting in a significant decrease in the waterproofing performance of the joint under cycle loading.

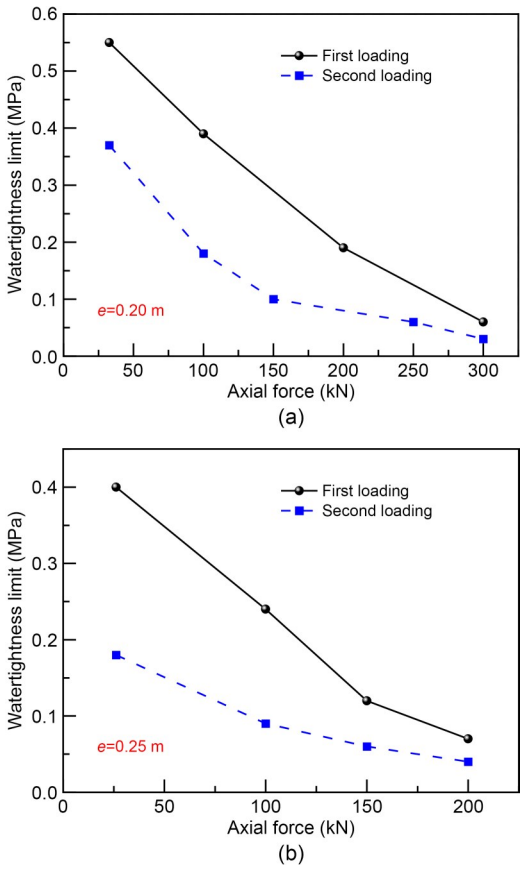

Fig. 17 Watertightness limit-axial force relationship of a joint during one cycle of loading in: (a) Case 2 (e=0.20 m); (b) Case 3 (e=0.25 m)

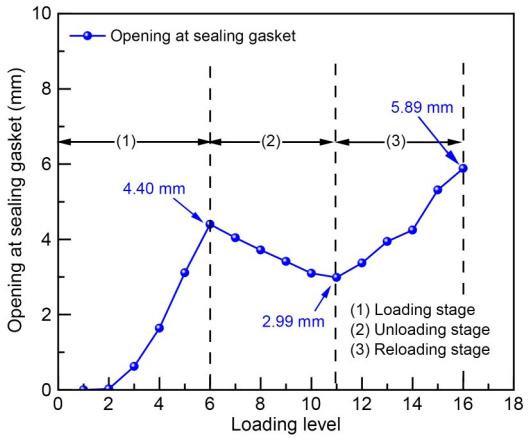

Fig. 18 Deformation-loading level relationship of the joint during one cycle of loading

(2) Waterproofing tests using the same set of tunnel segments revealed that the locations of leakage during the loading-unloading-reloading process were essentially consistent. The pressurized water consistently flowed out through the path with the weakest waterproofing capacity at the gasket-to-gasket interface (Fig. 16). This phenomenon indicates that the area experiencing water leakage becomes the weak link in the joint's waterproofing ability. The existing leakage paths in the joint during the early stages become "channels" for later leakage, contributing to the deterioration of the joint's waterproofing performance. Even if the joint no longer leaks due to the restoration of

external conditions, the weak link remains. Therefore, we conclude that the variation in waterproofing performance is largely related to the stress history of the gaskets that are subjected to external loads.

Our research results suggest that segmental tunnels may face great difficulty in repairing joint deformation and waterproofing capabilities following even one loading-unloading-reloading cycle. As a result, after experiencing surcharge, increased attention should be paid to tunnel leakage flaws even after unloading. To ensure that the gaskets are tightly compressed in the groove, the use of grouting and other methods should be prioritized to restore tunnel joint deformations.

3.3 Deformation of the sealing gasket

Essentially, external loads impact the joint's waterproofing performance by altering the deformation of the sealing gasket. The deformation of the sealing gasket is thus synchronized and controlled by the joint deformation. In this subsequent test, the deformation behavior of the joint and sealing gasket is investigated in terms of the extrados joint opening, intrados joint opening, and the opening at the sealing gasket. Taking Case 1 as an example, Fig. 19 depicts the development curves of the deformation increments. Δd_s, Δd_{ej}, and Δd_{ij} are opening deformations at the sealing gasket, extrados joint, and intrados joint, respectively. We can see that the extrados joint gradually opens, while the intrados joint undergoes compression, indicating a slight rotation in the segmental joint. Simultaneously, under the influence of joint rotation, the opening at the sealing gasket gradually enlarges. When the axial force was increased to 550 kN, the joint reached its ultimate waterproofing capability. Ultimately, the test was terminated when the segmented concrete at the joint intrados contact area suddenly was crushed.

To further investigate the deformation of the sealing gasket, we should first note that the compression of the sealing gasket is defined as:

$$C_g = t - d - \frac{\delta}{2}, \tag{2}$$

where t is the thickness of the sealing gasket (t=32 mm), d is the depth of the gasket groove, and δ is the joint opening at the sealing gasket. The principle of Eq. (2) is illustrated in Fig. 20. Fig. 21 depicts the development of the compression of the sealing gasket under different eccentricities before reaching the watertightness

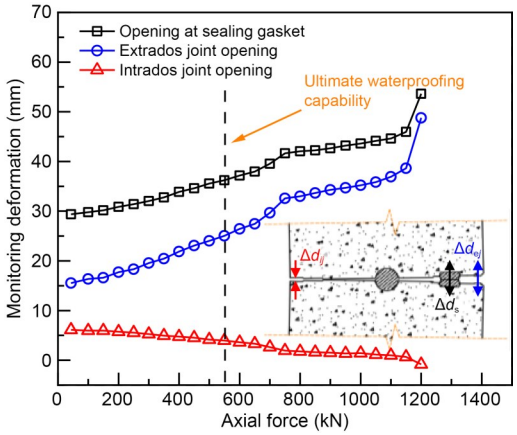

Fig. 19 Load-deformation relationship for the joint and the sealing gasket

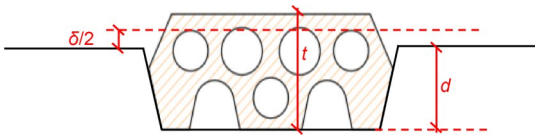

Fig. 20 Principle behind calculating the compression of the sealing gasket

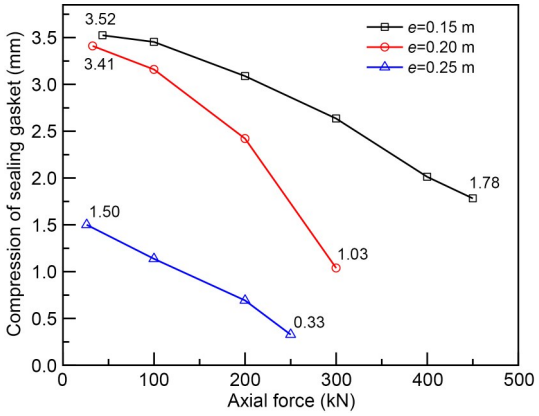

Fig. 21 Compression-load relationship of the sealing gasket under different eccentricities

limit. Note that the initial compression of the sealing gasket may differ due to manual assembly differences. However, under different eccentricities, the compression of the sealing gasket does show an accelerated decline as the axial force increases, which is attributed to the decline in the joint's flexural stiffness.

Through this test, the relationship between external loads and the deformation of the sealing gasket was revealed, showing that the deformation was primarily governed by joint rotation. The sealing gasket mainly exhibits a reduction in compression under external loads. This has also been confirmed by previous

studies (Gong et al., 2018; Wang and Huang, 2020), which showed that a reduction in compression of the sealing gasket was the main factor influencing waterproofing performance.

3.4 Effect of gasket deformation on waterproofing performance

To explore systematically the relationship between the compression of the sealing gasket and waterproofing performance, an analysis based on both theoretical results and experimental findings has been conducted. The waterproofing performance of the elastic sealing gasket is mainly determined by the contact stress between the gaskets. The waterproofing principle of the sealing gasket is shown in Fig. 22. Under the action of the confining stress P_c, external water pressure P_w, and contact stress P_{ge}, forces from these pressures are balanced (Eq. (3)). In a leakage situation, the external water pressure is greater than a critical water pressure (i.e. the watertightness limit P_{cw}) to flow through the sealing gasket. Based on the research by Robin (1973) and Walsh (1981), Eq. (4) was established to describe the watertightness limit (P_{cw}) under different degrees of opening and offset of the sealing gasket (also illustrated in Fig. 23). Herein, the sealing coefficients k_ε and k_s account for the influences of the opening and offset of the sealing gasket, respectively. The watertightness limit can be rewritten as Eq. (5) after substituting P_{cw} into Eq. (3). It is worth noting that P_{ge} is represented in terms of the elastic modulus (E) and strain (ε) in Eq. (5). The sealing coefficient is given by Eq. (6), in which ξ, κ, and λ are gasket parameters that can be easily determined from the test data.

$$P_c = P_w + P_{ge}, \tag{3}$$

$$P_{cw} = k_s k_\varepsilon P_c, \tag{4}$$

$$P_{cw} = \frac{k_s k_\varepsilon}{1 - k_s k_\varepsilon} E\varepsilon, \tag{5}$$

$$\begin{cases} k_s = \left(\dfrac{w_g - s}{w_g} \right)^{\xi}, \\ k_\varepsilon = \kappa\varepsilon + \lambda, \end{cases} \tag{6}$$

where k_ε and k_s are the coefficients that depend on the strain (ε) and offset (s) of the sealing gasket, respectively, and w_g is the width of the sealing gasket. In this test, it is assumed that there is no offset of the sealing gasket. Therefore, deriving from Eq. (5), the watertightness limit can be rewritten as Eq. (7):

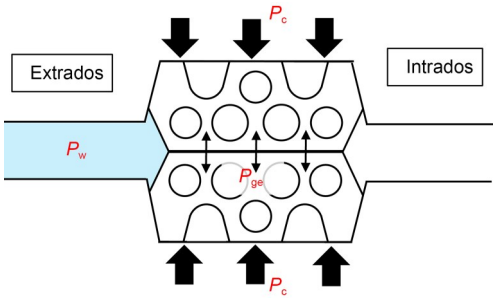

Fig. 22 Waterproofing principle of the sealing gasket

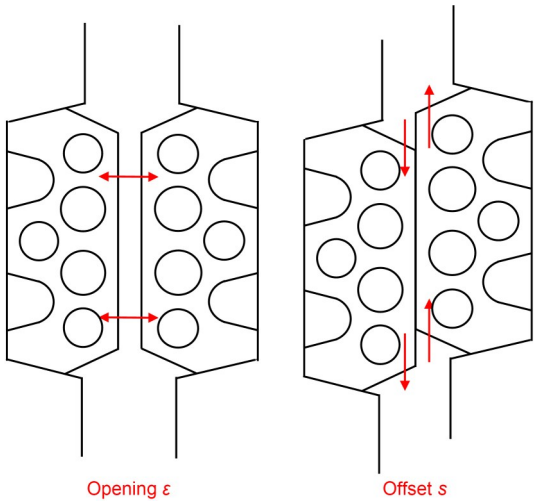

Fig. 23 Schematic of the sealing gasket deformation

$$P_{cw} = \frac{k_\varepsilon}{1 - k_\varepsilon} \cdot E\varepsilon. \tag{7}$$

According to research by Gong et al. (2018) and Wang and Huang (2020), the parameter values are as follows: E=1.66 MPa, κ=1.38, and λ=0.27. Then, the watertightness limit can be calculated by Eq. (7) with respect to the compression of the sealing gasket. Fig. 24 illustrates the development of theoretical and measured watertightness limit pressures for the three tested eccentricity values.

The experimental results indicate that the watertightness limit increases at an accelerating rate with the increased compression of the sealing gasket, which is consistent with previous studies (Gong et al., 2018; Wang and Huang, 2020; Zhang et al., 2022b). This is plausible because the contact forces at the different interfaces (such as the gasket-gasket or gasket-groove interface) increase with the compression of the sealing gasket. Consequently, water leakage becomes less likely as the compression increases.

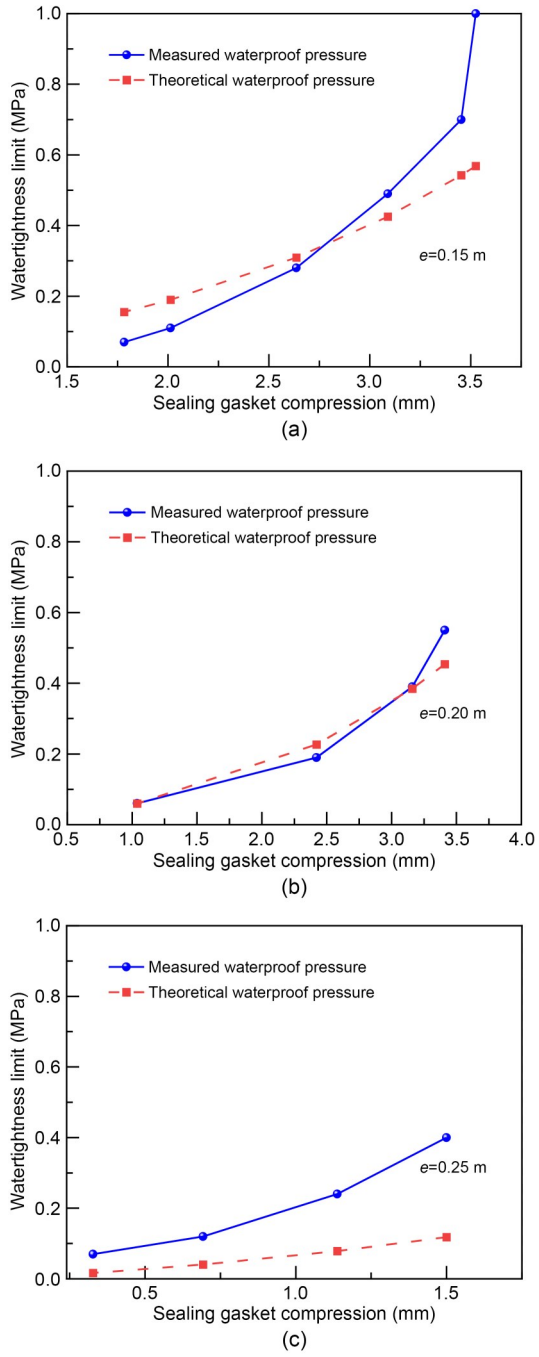

Fig. 24 Comparison between the results of measured and theoretical watertightness limits: (a) Case 1 (e=0.15 m); (b) Case 2 (e=0.20 m); (c) Case 3 (e=0.25 m)

The measured and theoretical watertightness limits were found to be relatively similar. However, the theoretical watertightness limit tends to be lower than the actual watertightness limit when the sealing gasket compression is considerable, suggesting that the theoretical predictions are conservative. In general, the theoretical approach only accounts for one potential leakage path, namely, the gasket-gasket interface. Therefore, as the sealing gasket becomes increasingly compressed, the theoretical approach shows a roughly linear growth in watertightness limit. This implies that the experimentally observed nonlinear acceleration of water leakage with increasing compression is not well described by the theoretical formulation.

Based on the above analysis, the impact of external loads on waterproofing performance can be summarized in two parts: (1) As the external loads increase, the compression of the sealing gasket declines at an accelerating rate; (2) As the compression of the gasket decreases, the waterproofing performance declines at an accelerated rate. However, part (1) has a more dominant impact. This is because the waterproofing performance of the joint experiences an accelerated decline as the external loads increase, as was discussed in Section 3.1 and shown in Fig. 15.

4 Conclusions

We investigated the influence of external loads on the waterproofing performance of longitudinal segmental joints through full-scale experiments. The effects of load magnitude, eccentricity, and loading-unloading-reloading cycles on waterproofing performance were accordingly revealed. Additionally, the correlations between the joint force, the deformation of sealing gasket, and the waterproofing performance were analyzed.

The joint's waterproofing performance was found to be significantly impacted by the magnitude of the external load and the bending moment. Our results indicate that the watertightness limit dramatically decreases as the external load and bending moment increase, particularly in the early stages of loading (N< 200 kN). The joints exhibiting initial leakage were extremely sensitive to external loads, approaching their watertightness limit with only a 100 Pa increase in water pressure.

It was also shown that even one loading cycle can considerably decrease a joint's waterproofing performance. Only about half of the watertightness limit during initial loading was retained during the reloading process. The primary cause of this is the irreversible deformation of the sealing gasket and the development of weak points during the loading cycle.

Under external loads, the extrados joint gradually opens, while the intrados joint undergoes compression, indicating that the segmental joint rotates. It was also observed that an increase in external load accelerates the joint's rotation, causing the compression of the sealing gasket to rapidly decrease. This is the primary reason why segmental tunnel joints leak under external loads.

Based on both theoretical and experimental results, as the compression of the sealing gasket increases, the watertightness limit increases rapidly. Nevertheless, the theoretical approach only accounts for one potential leakage path, which is the gasket-gasket interface. Therefore, the rapid change in watertightness limit with the compression of the sealing gasket is difficult for theoretical formulations to describe.

The findings of this study can support segmental tunnel waterproofing design, potentially bolstering safety and longevity in the face of effects from surcharge and unloading. Nonetheless, we should note that in these tests, the stress and deformation of the joints were mainly approximated by bending moments. In practice, the joint located along the springline is subjected to lateral soil pressure, which might limit the development of the lateral opening. Thus, the conditions of our waterproofing experiments may not fully reflect the complicated scenarios experienced in real underground situations. As a result, future study might investigate the impact of lateral pressures and utilize more sophisticated forms for the sealing gaskets.

Acknowledgments

This work is supported by the National Key Research and Development Program of China (No. 2022YFC3800905), the National Natural Science Foundation of China (Nos. 52238010, 52090082, and 52108381), the Shanghai Science and Technology Committee Program (Nos. 22XD1430200, 23DZ1202806, and 21DZ1200601), the Young Elite Scientists Sponsorship Program by the China Association for Science and Technology (No. 2023QNRC001), and the Fundamental Research Funds for the Central Universities, China.

Author contributions

Dongmei ZHANG designed the research. Sirui CHEN wrote the first draft of the manuscript. Sirui CHEN and Zhaoyuan ZHANG processed the experimental data. Zhongkai HUANG helped to organize the manuscript. Dongmei ZHANG and Zhongkai HUANG revised and edited the final version. Long SU provided resources and project administration.

Conflict of interest

Dongmei ZHANG, Sirui CHEN, Zhongkai HUANG, Zhaoyuan ZHANG, and Long SU declare that they have no conflict of interest.

References

Chen RP, Meng FY, Li ZC, et al., 2016. Investigation of response of metro tunnels due to adjacent large excavation and protective measures in soft soils. *Tunnelling and Underground Space Technology*, 58:224-235. https://doi.org/10.1016/j.tust.2016.06.002

Ding WQ, Gong CJ, Mosalam KM, et al., 2017. Development and application of the integrated sealant test apparatus for sealing gaskets in tunnel segmental joints. *Tunnelling and Underground Space Technology*, 63:54-68. https://doi.org/10.1016/j.tust.2016.12.008

Gong CJ, Ding WQ, Mosalam KM, et al., 2017. Comparison of the structural behavior of reinforced concrete and steel fiber reinforced concrete tunnel segmental joints. *Tunnelling and Underground Space Technology*, 68:38-57. https://doi.org/10.1016/j.tust.2017.05.010

Gong CJ, Ding WQ, Soga K, et al., 2018. Sealant behavior of gasketed segmental joints in shield tunnels: an experimental and numerical study. *Tunnelling and Underground Space Technology*, 77:127-141. https://doi.org/10.1016/j.tust.2018.03.029

Gong CJ, Ding WQ, Soga K, et al., 2019. Failure mechanism of joint waterproofing in precast segmental tunnel linings. *Tunnelling and Underground Space Technology*, 84:334-352. https://doi.org/10.1016/j.tust.2018.11.003

Gong CJ, Wang YY, Ding WQ, et al., 2022. Waterproof performance of sealing gasket in shield tunnel: a review. *Applied Sciences*, 12(9):4556. https://doi.org/10.3390/app12094556

Huang HW, Shao H, Zhang DM, et al., 2017. Deformational responses of operated shield tunnel to extreme surcharge: a case study. *Structure and Infrastructure Engineering*, 13(3):345-360. https://doi.org/10.1080/15732479.2016.1170156

Huang HW, Li QT, Zhang DM, 2018. Deep learning based image recognition for crack and leakage defects of metro shield tunnel. *Tunnelling and Underground Space Technology*, 77:166-176. https://doi.org/10.1016/j.tust.2018.04.002

Huang ZK, Pitilakis K, Argyroudis S, et al., 2021. Selection of optimal intensity measures for fragility assessment of circular tunnels in soft soil deposits. *Soil Dynamics and Earthquake Engineering*, 145:106724. https://doi.org/10.1016/j.soildyn.2021.106724

Huang ZK, Cheng YX, Zhang DM, et al., 2024. Seismic fragility and resilience assessment of shallowly buried large-section underground civil defense structure in soft soils: framework and application. *Tunnelling and Underground Space Technology*, 146:105640. https://doi.org/10.1016/j.tust.2024.105640

Kasper T, Meschke G, 2006. A numerical study of the effect of soil and grout material properties and cover depth in

shield tunnelling. *Computers and Geotechnics*, 33(4-5): 234-247.
https://doi.org/10.1016/j.compgeo.2006.04.004

Koyoma Y, Nishimura T, 1998. The design of lining segment of shield tunnel using a beam-spring model. *Quarterly Report of RTRI (Railway Technical Research Institute)*, 39(1):23-27.

Lee KM, Ge XW, 2001. The equivalence of a jointed shield-driven tunnel lining to a continuous ring structure. *Canadian Geotechnical Journal*, 38(3):461-483.
https://doi.org/10.1139/cgj-38-3-461

Li RJ, Gong CJ, Ding WQ, 2023. Aging performance under assembly pressure of joint gasket in shield tunnel. *Journal of Railway Science and Engineering*, 20(5):1786-1799 (in Chinese).
https://doi.org/10.19713/j.cnki.43-1423/u.T20222226

Li SH, Zhang MJ, Li PF, 2021. Analytical solutions to ground settlement induced by ground loss and construction loadings during curved shield tunneling. *Journal of Zhejiang University-SCIENCE A (Applied Physics & Engineering)*, 22(4):296-313.
https://doi.org/10.1631/jzus.A2000120

Lin XT, Chen XS, Su D, et al., 2022. An analytical model to evaluate the resilience of shield tunnel linings considering multistage disturbances and recoveries. *Tunnelling and Underground Space Technology*, 127:104581.
https://doi.org/10.1016/j.tust.2022.104581

Liu X, Bai Y, Yuan Y, et al., 2016. Experimental investigation of the ultimate bearing capacity of continuously jointed segmental tunnel linings. *Structure and Infrastructure Engineering*, 12(10):1364-1379.
https://doi.org/10.1080/15732479.2015.1117115

MHURD (Ministry of Housing and Urban-Rural Development of the People's Republic of China), 2010. Code for Design of Concrete Structures. GB/T 50010-2010, National Standards of the People's Republic of China (in Chinese).

Petraroia DN, Plückelmann S, Mark P, et al., 2024. Tunnel lining segments with enhanced bearing capacity using hybrid concrete concepts. *Tunnelling and Underground Space Technology*, 143:105484.
https://doi.org/10.1016/j.tust.2023.105484

Robin PYF, 1973. Note on effective pressure. *Journal of Geophysical Research*, 78(14):2434-2437.
https://doi.org/10.1029/JB078i014p02434

Shalabi FI, Cording EJ, Paul SL, 2012. Concrete segment tunnel lining sealant performance under earthquake loading. *Tunnelling and Underground Space Technology*, 31:51-60.
https://doi.org/10.1016/j.tust.2012.04.006

Shalabi FI, Cording EJ, Paul SL, 2016. Sealant behavior of gasketed segmental tunnel lining–Conceptual model. *Geomechanics and Tunnelling*, 9(4):345-355.
https://doi.org/10.1002/geot.201500030

Shen SL, Wu HN, Cui YJ, et al., 2014. Long-term settlement behaviour of metro tunnels in the soft deposits of Shanghai. *Tunnelling and Underground Space Technology*, 40:309-323.
https://doi.org/10.1016/j.tust.2013.10.013

Walsh JB, 1981. Effect of pore pressure and confining pressure on fracture permeability. *International Journal of Rock Mechanics and Mining Sciences & Geomechanics Abstracts*, 18(5):429-435.
https://doi.org/10.1016/0148-9062(81)90006-1

Wang FY, Huang HW, 2020. Theoretical analysis of the joint leakage in shield tunnel considering the typical deformation mode. *International Journal of Geomechanics*, 20(12): 04020218.
https://doi.org/10.1061/(asce)gm.1943-5622.0001861

Wang ZN, Shen SL, Zhou AN, et al., 2021. Investigation of time-dependent characteristics of EPDM rubber gasket used for shield tunnels. *Journal of Materials in Civil Engineering*, 33(9).
https://doi.org/10.1061/(asce)mt.1943-5533.0003844

Wu HN, Shen SL, Chen RP, et al., 2020. Three-dimensional numerical modelling on localised leakage in segmental lining of shield tunnels. *Computers and Geotechnics*, 122:103549.
https://doi.org/10.1016/j.compgeo.2020.103549

Wu HN, Liu L, Liu Y, et al., 2023. Weakening behavior of waterproof performance in joints of shield tunnels under adjacent constructions. *Frontiers of Structural and Civil Engineering*, 17(6):884-900.
https://doi.org/10.1007/s11709-022-0912-3

Xu BT, Qiu JF, Sun Q, et al., 2016. Study of the damage mechanics and dewatering recovery programs for the shield tunnel under the Yangtze river. *Environmental & Engineering Geoscience*, 22(4):352-366.
https://doi.org/10.2113/gseegeosci.22.4.352

Yang C, Shen SL, Hou DW, et al., 2018. Material properties of the seal gasket for shield tunnels: a review. *Construction and Building Materials*, 191:877-890.
https://doi.org/10.1016/j.conbuildmat.2018.10.021

Zhang DM, Ma LX, Zhang J, et al., 2015. Ground and tunnel responses induced by partial leakage in saturated clay with anisotropic permeability. *Engineering Geology*, 189: 104-115.
https://doi.org/10.1016/j.enggeo.2015.02.005

Zhang DM, Gao CP, Yin ZY, 2019. CFD-DEM modeling of seepage erosion around shield tunnels. *Tunnelling and Underground Space Technology*, 83:60-72.
https://doi.org/10.1016/j.tust.2018.09.017

Zhang DM, Bu XH, Pang J, et al., 2022a. Soil effect on the bearing capacity of a double-lining structure under internal water pressure. *Journal of Zhejiang University-SCIENCE A (Applied Physics & Engineering)*, 23(11):863-881.
https://doi.org/10.1631/jzus.A2200215

Zhang DM, Liu J, Huang ZK, et al., 2022b. Waterproof performance of tunnel segmental joints under different deformation conditions. *Tunnelling and Underground Space Technology*, 123:104437.
https://doi.org/10.1016/j.tust.2022.104437

Zhang GL, Zhang WJ, Li HL, et al., 2021a. Waterproofing behavior of sealing gaskets for circumferential joints in shield tunnels: a full-scale experimental investigation. *Tunnelling and Underground Space Technology*, 108:103682.
https://doi.org/10.1016/j.tust.2020.103682

Zhang GL, Zhang WJ, Cao WZ, et al., 2021b. A novel test setup for determining waterproof performance of rubber gaskets

used in tunnel segmental joints: development and application. *Tunnelling and Underground Space Technology*, 115:104079. https://doi.org/10.1016/j.tust.2021.104079

Zhang ZX, Sun J, Zhu YF, et al., 2018. Experimental study on waterproof performance of joint seal for deeply-buried storage and drainage tunnel. *Journal of Zhejiang University (Engineering Science)*, 52(3):431-439 (in Chinese). https://doi.org/10.3785/j.issn.1008-973X.2018.03.003

Zhao HL, Liu X, Bao YH, et al., 2017. Nonlinear simulation of tunnel linings with a simplified numerical modelling. *Structural Engineering and Mechanics*, 61(5):593-603. https://doi.org/10.12989/sem.2017.61.5.593

Zheng G, Cui T, Cheng XS, et al., 2017. Study of the collapse mechanism of shield tunnels due to the failure of segments in sandy ground. *Engineering Failure Analysis*, 79:464-490. https://doi.org/10.1016/j.engfailanal.2017.04.030

Zhou WF, Liao SM, Men YQ, 2021. A fluid-solid coupled modeling on water seepage through gasketed joint of segmented tunnels. *Tunnelling and Underground Space Technology*, 114:104008. https://doi.org/10.1016/j.tust.2021.104008